

Photophysical Properties and Electronic Structure of Stable, Tunable Synthetic Bacteriochlorins: Extending the Features of Native Photosynthetic Pigments

Eunkyung Yang,[†] Christine Kirmaier,[†] Michael Krayer,[‡] Masahiko Taniguchi,[‡] Han-Je Kim,[‡] James R. Diers,[§] David F. Bocian,^{*,§} Jonathan S. Lindsey,^{*,†} and Dewey Holten^{*,†}

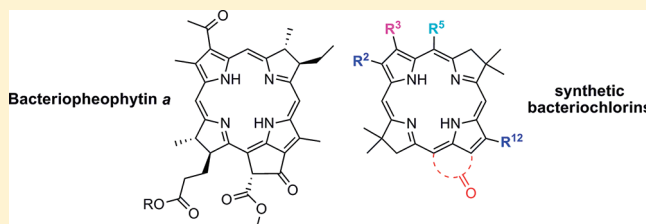
[†]Department of Chemistry, Washington University, St. Louis, Missouri 63130-4889, United States

[‡]Department of Chemistry, North Carolina State University, Raleigh, North Carolina 27695-8204, United States

[§]Department of Chemistry, University of California, Riverside, California 92521-0403, United States

 Supporting Information

ABSTRACT: Bacteriochlorins, which are tetrapyrrole macrocycles with two reduced pyrrole rings, are Nature's near-infrared (NIR) absorbers (700–900 nm). The strong absorption in the NIR region renders bacteriochlorins excellent candidates for a variety of applications including solar light harvesting, flow cytometry, molecular imaging, and photodynamic therapy. Natural bacteriochlorins are inherently unstable due to oxidative conversion to the chlorin (one reduced pyrrole ring) or the porphyrin. The natural pigments are also only modestly amenable to synthetic manipulation, owing to a nearly full complement of substituents on the macrocycle. Recently, a new synthetic methodology has afforded access to stable synthetic bacteriochlorins wherein a wide variety of substituents can be appended to the macrocycle at preselected locations. Herein, the spectroscopic and photophysical properties of 33 synthetic bacteriochlorins are investigated. The NIR absorption bands of the chromophores range from ~700 to ~820 nm; the lifetimes of the lowest excited singlet state range from ~2 to ~6 ns; the fluorescence quantum yields range from ~0.05 to ~0.25; and the yield of the lowest triplet excited state is ~0.5. The spectroscopic/photophysical studies of the bacteriochlorins are accompanied by density functional theory (DFT) calculations that probe the characteristics of the frontier molecular orbitals. The DFT calculations indicate that the impact of substituents on the spectral properties of the molecules derives primarily from effects on the lowest unoccupied molecular orbital. Collectively, the studies show how the palette of synthetic bacteriochlorins extends the properties of the native photosynthetic pigments (bacteriochlorophylls). The studies have also elucidated design principles for tuning the spectral and photophysical characteristics as required for a wide variety of photochemical applications.



INTRODUCTION

The centrality of chlorophylls in plant photosynthesis is well appreciated and has led to numerous studies of the spectroscopic and photophysical properties of chlorophylls and their synthetic analogues. Less studied but equally important are the bacteriochlorophylls, which underpin bacterial photosynthesis. Bacteriochlorophylls are tetrahydroporphyrins wherein two reduced pyrrole rings are located at opposite sides of the macrocycle, to be compared with the single reduced ring of chlorophylls (which are dihydroporphyrins). The structures of bacteriochlorophylls *a*, *b*, and *g* are shown in Chart 1 (bacteriochlorophylls *c–f* contain the dihydroporphyrin chromophore and hence are misnamed). The increased saturation of the macrocycle leads to strong absorption in the near-infrared (NIR) spectral region: bacteriochlorophylls *a*, *b*, and *g* (in dioxane) absorb at 772, 794, and 762 nm, respectively, to be compared with absorption at 662 and 644 nm for chlorophylls *a* and *b*.¹

Two major impediments to studies of bacteriochlorophylls have entailed (i) instability of the naturally occurring macrocycles

(including susceptibility toward adventitious dehydrogenation thereby forming the corresponding chlorin)² and (ii) a nearly full complement of substituents about the perimeter of the macrocycles, thereby limiting semisynthetic transformations.^{3,4} Synthetic bacteriochlorins in principle offer an attractive alternative to the bacteriochlorins derived semisynthetically from bacteriochlorophylls. Traditional methods for the synthesis of bacteriochlorins involve subjecting a chlorin or porphyrin to hydrogenation or addition (e.g., vicinal dihydroxylation).⁵ While operationally simple, both methods can yield regioisomers depending on the substituents about the perimeter of the macrocycle, and the former method leaves the bacteriochlorin susceptible to aerobic dehydrogenation.

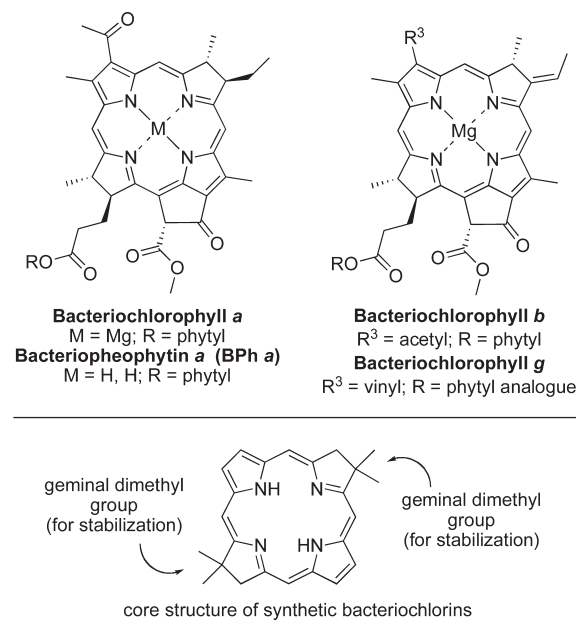
The limited bacteriochlorin architectures available have precluded addressing a number of fundamental questions concerning

Received: June 4, 2011

Revised: August 2, 2011

Published: August 29, 2011

Chart 1. Naturally Occurring Bacteriochlorophylls (Top) and Synthetic Bacteriochlorins (Bottom)



the relation between molecular structure and photophysical features. Chief among the structural questions are the effects of substituents arrayed about the perimeter of the macrocycle (including the presence of the isocyclic ring and variants thereof) on the spectra and photophysical properties. Because bacteriochlorophylls are Nature's NIR absorbers par excellence, a related question concerns the extent to which synthetic manipulations can shift the long-wavelength absorption band deeper into the NIR while retaining a singlet excited-state lifetime of sufficient duration for viable photochemical reactions. The position of the long-wavelength absorption band is important not only with regards to light-harvesting but also establishes an upper limit on the energy level of the first singlet excited state. Finally, it warrants emphasis that photosynthetic phenomena stem from large numbers of pigments working in concert. In that regard, synthetic multichromophore arrays have been widely used to good effect to delineate molecular factors that affect electron-transfer and energy-transfer phenomena. Such arrays have largely employed porphyrins and to a lesser extent chlorins despite the absence of NIR absorption for both types of chromophores.⁶ Very few synthetic arrays have incorporated bacteriochlorins.⁷ Indeed, the studies to date of bacteriochlorins tend to encompass the bacteriochlorophylls either as monomers or as part of natural protein assemblies.⁸ Thus, a large body of important studies concerning bacteriochlorins has remained unaddressed.

In addition to fundamental studies, bacteriochlorins are of interest for a number of applications wherein capture of NIR light is of paramount importance. Exemplary applications include (i) bioinspired solar energy conversion, given the abundance of solar radiation in the NIR region;⁹ (ii) polychromatic flow cytometry, given the dearth of spectroscopically distinct fluorescent markers in the virtually unexplored NIR region, thereby complementing the numerous markers for the visible spectral region;^{10,11} and (iii) molecular imaging^{11–19} and photodynamic therapy (PDT),^{3,4,12,19–26} given the deep penetration in soft tissue afforded by NIR light. Porphyrins annulated with conjugated

rings have recently been found to shift the long-wavelength absorption band into the NIR,^{27,28} but in one case that has been studied, the excited-state lifetime was dramatically shortened (to ~ 13 ps).²⁸ Maintaining a singlet excited-state lifetime of reasonable magnitude (≥ 1 ns) is important for achieving a number of efficient photochemical processes such as energy transfer and electron transfer.

To gain access to stable bacteriochlorins and retain the synthetic versatility required to address fundamental questions and diverse applications, we have been working to develop a de novo synthesis that affords bacteriochlorins equipped with a geminal dimethyl group in both reduced rings. The geminal dimethyl group blocks adventitious dehydrogenation and thereby affords a stable tetrahydroporphyrin chromophore. The core structure of the synthetic bacteriochlorins is shown in Chart 1. Synthetic manipulations have provided access to bacteriochlorins bearing diverse substituents at the 2,3,12,13 positions. One such class of bacteriochlorins also contains a methoxy group at the 5-position (termed "MeOBC" series), whereas a second class lacks the 5-methoxy substituent (termed "HBC" series). Table 1 shows 10 members of the former class and 17 members of the latter class. Further synthetic transformations have provided access to six bacteriochlorins wherein the 15-substituent is altered, affording three distinct classes as shown in Table 2. The classes include the "15-substituted" series and two series wherein a fifth ring has been annulated to the macrocycle. The rings include the five-membered isocyclic ring characteristic of naturally occurring bacteriochlorophylls (i.e., a bacterio-13¹-oxophorbine) and a six-membered imide ring (bacteriochlorin-13,15-dicarboximide) for which there are no natural counterparts. The imide motif has been accessed in (bacterio)chlorophyll chemistry (by base-mediated treatment of the natural macrocycles) as a means of achieving a more stable construct with bathochromically shifted absorption.

Herein, we first describe the spectral properties of the 33 synthetic bacteriochlorins shown in Tables 1 and 2. The synthesis of all compounds except one (see Supporting Information) have been reported.^{29–36} The compounds exhibit a range of long-wavelength absorption that spans 709–818 nm. We report measurements of the singlet excited-state lifetime, triplet excited-state lifetime, and quantum yields of all three decay processes of the singlet excited state (fluorescence, intersystem crossing, and internal conversion), from which the rate constants for these fundamental processes are derived. Density functional theoretical calculations have been carried out to assess the energy and composition of the four frontier molecular orbitals. Finally, we draw insights concerning the relation between diverse substituents in various patterns, observed spectral and photophysical properties, and molecular orbital characteristics. Taken together, the studies provide a foundation for the rational design of bacteriochlorin-containing molecular architectures that capture NIR light.

■ EXPERIMENTAL METHODS

1. Photophysical Measurements. Static and time-resolved photophysical measurements were performed as described previously.³⁷ Measurement of the fluorescence (Φ_f) and triplet excited-state (Φ_{isc}) quantum yields and singlet (τ_s) and triplet (τ_t) lifetimes utilized, unless noted otherwise, dilute (μM) Ar-purged toluene solutions at room temperature. Samples for Φ_f measurements had an absorbance <0.12 at the excitation wavelength. The Φ_f values were generally determined with respect to two standards and the results averaged. The standards

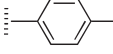
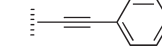
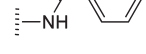
Table 1. Structures of Bacteriochlorins with Substituents at the 2,3,12,13-Positions

	ref	R ²	R ¹²	R ³	R ¹³
HBC Series					
HBC-H	32	H	H	H	H
HBC-Swt^{2,12}	33	Swt	Swt	H	H
HBC-M^{3,13}	31	H	H	M	M
HBC-Re^{3,13}	34	H	H	Re	Re
HBC-F³	34	H	H	F	H
HBC-T^{2,12}	29	T	T	H	H
HBC-P^{3,13}	32	H	H	P	P
HBC-C^{3,13}	34	H	H	C	C
HBC-CN^{3,13}	34	H	H	CN	CN
HBC-V^{3,13}	32	H	H	V	V
HBC-MEs^{3,13}	34	H	H	MEs	MEs
HBC-Me^{2,12}EEs^{3,13}	35	Me	Me	EEs	EEs
HBC-Et^{2,12}EEs^{3,13}	35	Et	Et	EEs	EEs
HBC-PE^{3,13}	32	H	H	PE	PE
HBC-T^{2,12}EEs^{3,13}	see SI	T	T	EEs	EEs
HBC-A^{3,13}	32	H	H	A	A
HBC-F^{3,13}	32	F	H	F	F
MeOBC series					
MeOBC-H	35	H	H	H	H
MeOBC-T^{2,12}	29	T	T	H	H
MeOBC-Py^{3,13}	35	H	H	Py	Py
MeOBC-EEs^{3,13}	35	H	H	EEs	EEs
MeOBC-Me^{2,12}EEs^{3,13}	35	Me	Me	EEs	EEs
MeOBC-Et^{2,12}EEs^{3,13}	35	Et	Et	EEs	EEs
MeOBC-A^{3,13}	36	H	H	A	A
MeOBC-Me^{2,12}A^{3,13}	36	Me	Me	A	A
MeOBC-An^{2,12}EEs^{3,13}	35	An	An	EEs	EEs
MeOBC-EEs^{2,3,12,13}	35	EEs	EEs	EEs	EEs
<i>p</i> -tolyl (T)					
phenyl (P)					
mesityl (M)					
4-pyridyl (Py)					
4-methoxyphenyl (An)					
3,5-dihydroxyphenyl (Re)					
1,5-dimethoxypent-3-yl (Swt)					
methyl (Me)					
ethyl (Et)					
vinyl (V)					
cyano (CN)					
carboxyl (C)					
formyl (F)					
acetyl (A)					
methyl ester (MEs)					
ethyl ester (EEs)					
phenylethyanyl (PE)					

(deoxygenated solutions) were (1) free base *meso*-tetraphenylporphyrin (**FbTPP**) in nondegassed toluene, for which $\Phi_f = 0.070$ was established with respect to the zinc chelate **ZnTPP** in nondegassed toluene ($\Phi_f = 0.030$),³⁸ consistent with prior

results on **FbTPP**,³⁹ and (2) 8,8,18,18-tetramethylbacteriochlorin³² in Ar-purged toluene, for which $\Phi_f = 0.14$ was established with respect to **FbTPP** and chlorophyll *a* (**Chl a**) in deoxygenated benzene⁴⁰ ($\Phi_f = 0.325$).

Table 2. Structures of Bacteriochlorins, Bacteriochlorinimides, and Bacteriooxophorbine

	ref	R ²	R ¹²	R ³	R ¹³	R ⁵	R ¹⁵								
15-substituted series															
MeOBC-OMe ¹⁵	35	H	H	H	H	OMe	OMe								
MeOBC-T ^{2,12} Bza ¹⁵	30	T	T	H	H	OMe	Bza								
MeOBC-T ^{2,12} PE ¹⁵	30	T	T	H	H	OMe	PE								
Bacteriooxophorbine															
MeOBOP	36	Me	Me	A	—	OMe	—								
Bacteriochlorinimides															
MeOBC-I	36	Et	Et	EEs	—	OMe	—								
HBC-I	36	Et	Et	EEs	—	H	—								
	p-tolyl (T)		methyl (Me)		ethyl (Et)		ethyl ester (EEs)		acetyl (A)		phenylethylnyl (PE)		N-Benzamido (Bza)		methoxy (OMe)

The τ_s value for each bacteriochlorin was first probed using a time-correlated single photon counting (TCSPC) instrument that employed Soret excitation flashes derived from a nitrogen-pumped dye laser (PTI LaserStrobe) and a Gaussian instrument response function of 0.6 ns. The values were in good agreement with those obtained for select compounds using a fluorescence modulation technique (Spex Tau2).⁴¹

The Φ_{isc} values were obtained using a transient-absorption technique in which the extent of bleaching of the ground-state $Q(1,0)$ band due to the lowest singlet excited state was measured immediately following a 130 fs flash in the $Q_y(0,0)$ band and compared with bleaching due to formation of the lowest triplet excited state at the asymptote of the singlet excited-state decay.³⁷ The bleaching signals are referenced to a relatively featureless Q_x -region transient absorption that is generally not substantially different for the S_1 and S_0 excited states of the free base bacteriochlorins.

2. Density Functional Theory Calculations. DFT calculations were performed with Spartan '08 for Windows version 1.2.0 in parallel mode⁴² on a PC equipped with an Intel i7-975 CPU, 24 GB ram, and three 300 GB, 10k rpm hard drives. The hybrid B3LYP functional and the LACVP basis set were employed. The equilibrium geometries were fully optimized using the default parameters of the Spartan '08 program.

■ RESULTS

1. Absorption Spectra. Electronic ground-state absorption spectra of representative bacteriochlorins are shown in Figure 1. The absorption spectrum of each bacteriochlorin contains four

main features with maxima in the following spectral ranges: $B_y(0,0)$ (340–371 nm), $B_x(0,0)$ (357–408 nm), $Q_x(0,0)$ (489–550 nm), and $Q_y(0,0)$ (707–818 nm). For each of these four origin bands, a weaker (1,0) vibronic satellite feature can be seen roughly 1300 cm⁻¹ to higher energy. [Note that both the nominal B_x and B_y bands may have contributions from x - and y -polarized transitions and for some bacteriochlorins are substantially spectrally overlapped.] The $Q_y(0,0)$ bands have a full width at half-maximum (fwhm) in the range 11–25 nm. The absorption characteristics of all the synthetic bacteriochlorins along with those of the natural photosynthetic pigment bacteriopheophytin *a* (**BPh a**) are listed in Table 3.

The $Q_y(0,0)$ band is of interest because it represents absorption of light to produce the lowest singlet excited state, which is key to much of the photophysical behavior. The two bacteriochlorinimides have $Q_y(0,0)$ bands at the longer wavelength (lower energy) end of the range: **HBC-I** (818 nm) and **MeOBC-I** (793 nm). The two analogues that have no substituents at the β -pyrrole positions absorb near the shorter wavelength end of the range: **HBC-H** (713 nm) and **MeOBC-H** (709 nm). Other analogues, such as those bearing 3,13-diacetyl groups, absorb at intermediate wavelengths: **HBC-A**^{3,13} (768 nm) and **MeOBC-A**^{3,13} (740 nm). These pairs of compounds also illustrate the effect of the 5-OMe group to modestly shift the $Q_y(0,0)$ band hypsochromically compared to analogues bearing a 5-hydrogen substituent (Table 3).

Because of uncertainties associated with determination of molecular absorption (extinction) coefficients (e.g., weighing small amounts of material), it has been common in the literature

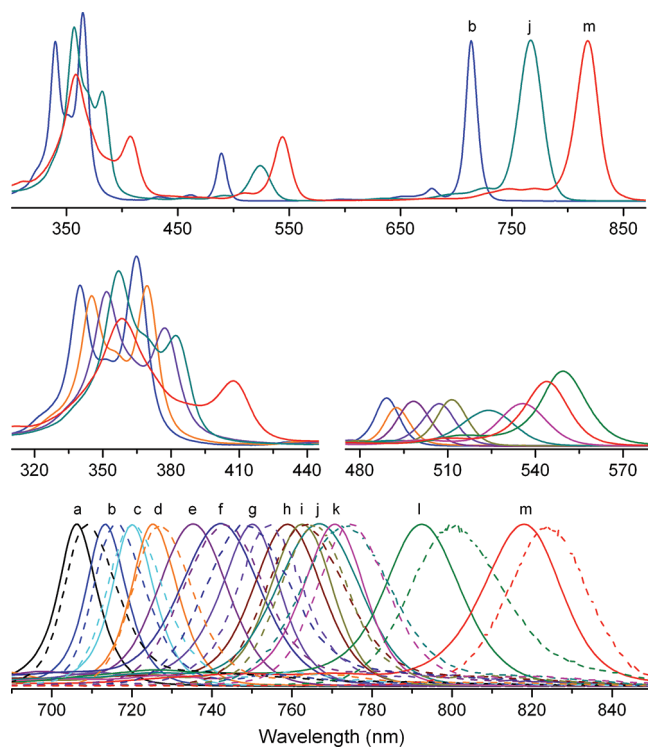


Figure 1. Absorption (— solid lines) and emission (--- dashed lines) spectra in toluene at room temperature of bacteriochlorins (normalized at the $Q_y(0,0)$ absorption bands); (top) entire spectra, (middle left) magnification of the Soret (B_x and B_y) region, (middle right) magnification of the Q_x region, and (bottom) magnification of the Q_y region. The labels in the bottom and top panels and the colors in all panels are as follows: MeOBC-OMe¹⁵ (a, black), HBC-H (b, blue), HBC-Swt^{2,12} (c, cyan), HBC-M^{3,13} (d, orange), HBC-P^{3,13} (e, purple), MeOBC-Me^{2,12}A^{3,13} (f, royal), HBC-V^{3,13} (g, violet), MeOBC-EEs^{2,3,12,13} (h, wine), HBC-PE^{3,13} (i, dark yellow), HBC-T^{2,12}EEs^{3,13} (j, dark cyan), HBC-F^{3,13} (k, magenta), MeOBC-I (l, olive), and HBC-I (m, red).

on photosynthetic pigments (chlorophylls and bacteriochlorophylls) to examine how changes in molecular characteristics affect the intensity of the $Q_y(0,0)$ band relative to the Soret (B_y , B_x) maximum.⁴³ This peak-intensity ratio (I_{Q_y}/I_B) is listed in Table 3. It deserves mention that where molar absorption coefficients have been measured (e.g., MeOBC-T^{2,12} or HBC-T^{2,12}, $\epsilon_{Q_y} = 120\,000$ or $130\,000\,M^{-1}\,cm^{-1}$, respectively)²⁹ the magnitude is fully in line with those reported for naturally occurring bacteriochlorophylls.^{1,8} Because of variations in absorption bandwidths and in spectral overlap, trends in the oscillator strengths of the transitions are more faithfully gauged using integrated band intensities. For this purpose, Table 3 also includes the integrated intensity of the Q_y manifold [$Q_y(0,0) + Q_y(1,0)$ bands] relative to the integrated intensity of the entire B manifold [$B_y(0,0) + B_y(1,0) + B_x(0,0) + B_x(1,0)$ bands]. The table also lists analogous intensity ratios for the $Q_x(0,0)$ band relative to the $Q_x(1,0)$ band, which normally has a relatively constant extinction coefficient for a series of related tetrapyrroles (because its intensity is derived from vibronic borrowing with the B_x transition).

Figure 2A plots the Q_y/B integrated intensity ratio versus the $Q_y(0,0)$ energy (and wavelength). With the exception of the bacteriochlorinimides (HBC-I and MeOBC-I), there is a good linear relationship between these two quantities for all

the synthetic bacteriochlorins (and natural photosynthetic pigment BPh *a*). The greatest effect of the 5-OMe group on the intensity of the $Q_y(0,0)$ band occurs for bacteriochlorins containing a 3,13-dicarbonyl (acetyl, ester, imide) moiety, including a 30% increase for MeOBC-I versus HBC-I. These results are analyzed below in terms of the connection between the spectral properties and molecular orbital (MO) characteristics.

2. Fluorescence Spectra. The fluorescence emission spectra of representative bacteriochlorins in toluene are shown in Figure 1 (dashed lines). The fluorescence spectrum of each bacteriochlorin is dominated by the $Q_y(0,0)$ band, which is positioned on the average 4 nm to longer wavelength ($80\,cm^{-1}$ to lower energy) than the $Q_y(0,0)$ absorption maximum (Table 3). This rather small “Stokes” shift indicates little change in bacteriochlorin structure or solvent interactions upon photoexcitation. The $Q_y(0,0)$ fluorescence bands have a fwhm in the range 16–29 nm.

3. Fluorescence Quantum Yields and Singlet Excited-State Lifetimes. The fluorescence quantum yields (Φ_f) of the bacteriochlorins are in the range 0.04–0.25 with an average value of 0.15. The singlet excited-state lifetimes (τ_s) are in the range 1.9–6.2 ns with an average value of 3.8 ns. These values and other photophysical parameters are collected in Table 4.

Close examination of Table 4 reveals two trends: (i) The Φ_f and τ_s values modestly decrease as the $Q_y(0,0)$ absorption band shifts to longer wavelength (lower singlet excited-state energy). These trends are shown for representative bacteriochlorins in Figure 3. (ii) The average Φ_f and τ_s values for the bacteriochlorins containing a 5-OMe substituent (“MeOBC series”) (0.18, 4.3 ns) are modestly larger than those of the analogues bearing a 5-H substituent (“HBC series”) (0.13, 3.6 ns). The same is true for the respective bacteriochlorinimides (Table 4). These trends are illustrated by comparison of the λ_{Q_y} , Φ_f , and τ_s values for six representative compounds (and three 5-OMe versus 5-H pairs) in order of increasing $Q_y(0,0)$ wavelength (decreasing excited-state energy): MeOBC-H (709 nm, 0.25, 5.0 ns) > HBC-H (713 nm, 0.13, 4.0 ns) > MeOBC-A^{3,13} (740 nm, 0.14, 3.8 ns) > HBC-A^{3,13} (768 nm, 0.11, 2.9 ns) > MeOBC-I (793 nm, 0.05, 2.2 ns) > HBC-I (818 nm, 0.04, 1.9 ns). Similarly, the average Φ_f and τ_s values for the bacteriochlorins containing a 5-OMe substituent plus a 15-substituent (“15-substituted series”) (0.19, 5.4 ns) are modestly larger than those containing only a 5-OMe group (MeOBC series) (0.18, 4.3 ns). Selected members of these sets allow comparison of λ_{Q_y} , Φ_f , and τ_s values for bacteriochlorins containing 5,15-OMe, 5-OMe, and no OMe group: MeOBC-OMe¹⁵ (707 nm, 0.16, 6.2 ns) > MeOBC-H (709 nm, 0.25, 5.0 ns) > HBC-H (713 nm, 0.13, 4.0 ns). For comparison, typical (solvent-dependent) values for the native photosynthetic pigment BPh *a* are 750 nm, 0.10, and 2.7 ns (Table 4).⁴⁴

4. Yields and Lifetimes of the Triplet Excited State. The quantum yield of intersystem crossing from the lowest singlet excited state to the lowest triplet excited state (Φ_{isc}), commonly referred to as the triplet yield, is in the range 0.24–0.80. All but four of the 33 bacteriochlorins have triplet yields in the range 0.40–0.65 despite a substantial variation in the nature and pattern of substituents. Furthermore, the average value and standard deviation is 0.5 ± 0.1 for both the HBC series (17 compounds) and MeOBC series (10 compounds). These Φ_{isc} values of the synthetic bacteriochlorins are in general comparable to the value of 0.57 for BPh *a* (Table 4). On the other hand, the lifetimes of the lowest triplet excited state (τ_T) for

Table 3. Spectral Characteristics of Bacteriochlorins^a

compound	B _y (0,0) ^b	B _x (0,0) ^b	Q _x (0,0) ^c	Q _y (0,0) ^c	Q _y (0,0) ^d		Q _y (0,0) ^f		I _{Q_y} / _{I_B^h}	I _{Q_{x(0,0)}} / _{I_{Q_{x(1,0)}}ⁱ}	Σ_{Q_y}/Σ_B^j
	abs (nm)	abs (nm)	abs (nm)	abs (nm)	abs fwhm (nm)	em fwhm (nm)	ΔQ _y ^g abs-em (cm ⁻¹)				
HBC Series											
HBC-H	340	365	489	713	12	716	16	59	0.85	7.86	0.111
HBC-Swt ^{2,12}	344	364	492	720	13	722	17	38	1.00	6.09	0.122
HBC-M ^{3,13}	345	370	493	725	14	727	18	38	0.99	5.81	0.134
HBC-Re ^{3,13}	346	368	496	731	14	737	23	111	0.71	3.46	0.133
HBC-F ³	352	359	513	733	22	739	23	111	0.91	4.74	0.157
HBC-T ^{2,12}	351	374	499	736	20	742	23	110	1.00	6.11	0.143
HBC-P ^{3,13}	351	373	498	736	20	742	26	110	0.98	6.41	0.146
HBC-C ^{3,13 k}	344	371	506	734	19	737	20	55	0.76	5.48	0.135
HBC-CN ^{3,13}	347	372	515	748	14	752	17	71	1.33	10.2	0.156
HBC-V ^{3,13}	352	377	507	750	21	754	20	71	0.94	6.82	0.171
HBC-MEs ^{3,13}	352	377	523	754	17	757	19	53	1.06	7.83	0.165
HBC-Me ^{2,12} EEs ^{3,13}	354	384	520	760	19	764	20	69	0.98	8.20	0.186
HBC-Et ^{2,12} EEs ^{3,13}	354	383	521	761	20	764	21	52	0.94	8.32	0.165
HBC-PE ^{3,13}	363	380	511	763	18	766	20	51	1.72	8.60	0.173
HBC-T ^{2,12} EEs ^{3,13}	349	357	548	767	25	773	29	101	0.92	6.06	0.179
HBC-A ^{3,13}	360	389	533	768	19	771	20	51	1.19	5.84	0.194
HBC-F ^{3,13}	363	393	536	771	22	775	21	67	0.80	7.29	0.204
MeOBC Series											
MeOBC-H	345	367	501	709	11	711	18	40	0.87	8.07	0.112
MeOBC-T ^{2,12}	356	373	511	731	20	736	23	93	0.89	5.86	0.144
MeOBC-Py ^{3,13}	364	364	515	734	22	741	21	129	0.89	5.33	0.138
MeOBC-EEs ^{3,13}	355	375	525	735	20	740	24	92	1.01	6.10	0.142
MeOBC-Me ^{2,12} EEs ^{3,13}	357	380	520	738	18	741	21	55	0.96	6.48	0.129
MeOBC-Et ^{2,12} EEs ^{3,13}	357	379	521	739	18	741	21	37	1.10	6.50	0.149
MeOBC-A ^{3,13}	363	363	529	740	23	748	27	145	0.96	3.68	0.151
MeOBC-Me ^{2,12} A ^{3,13}	363	363	523	743	24	749	26	108	0.95	3.36	0.166
MeOBC-An ^{2,12} EEs ^{3,13}	360	376	527	749	23	755	26	106	1.09	5.99	0.164
MeOBC-EEs ^{2,3,12,13}	361	368	550	759	20	763	23	69	1.21	4.63	0.182
15-Substituted Series											
MeOBC-OMe ¹⁵	359	368	511	707	12	709	16	40	0.55	7.86	0.087
MeOBC-T ^{2,12} Bza ¹⁵	358	378	519	736	20	741	23	92	0.87	6.26	0.142
MeOBC-T ^{2,12} PE ¹⁵	387	387	551	754	22	759	24	87	0.95	3.92	0.145
Bacteriooxophorbine											
MeOBOP	359	376	530	733	19	739	26	111	0.93	4.89	0.138
Bacteriochlorinimides											
MeOBC-I	371	407	550	793	22	798	26	79	1.02	7.25	0.142
HBC-I	358	408	544	818	24	823	24	74	1.28	8.40	0.185
Standards											
BPh <i>a</i>	362	389	532	758	31	768	27	172	0.69	4.17	0.153

^a Obtained in toluene at room temperature unless noted otherwise. ^b The two Soret features are labeled B_x(0,0) and B_y(0,0), but the bands may be of mixed parentage. ^c Position (nm) of the Q_x(0,0) and Q_y(0,0) absorption bands. ^d Fwhm (in nm) of the Q_y(0,0) absorption band. ^e Position (nm) of the Q_y(0,0) fluorescence emission band. ^f Fwhm (in nm) of the Q_y(0,0) fluorescence band. ^g Difference in energy (cm⁻¹) between the peak positions of the Q_y(0,0) absorption and fluorescence bands. ^h Ratio of the peak intensities of the Q_y(0,0) band to the Soret (B) maximum, which could be either B_x(0,0) or B_y(0,0). ⁱ Ratio of the peak intensities of the Q_x(0,0) and Q_x(1,0) bands. ^j Ratio of the integrated intensities of the Q_y manifold [Q_y(0,0)+Q_y(1,0)] to the Soret manifold [B_y(0,0)+B_y(1,0)+B_x(0,0)+B_x(1,0)], for spectra plotted in cm⁻¹. ^k Spectra measured in methanol.

the synthetic bacteriochlorins (35–233 μs) are generally significantly longer than those (16–30 μs) for BPh *a* in several solvents (Table 4).⁴⁴

5. Excited-State Decay Pathways and Rate Constants. The observables τ_S, Φ_f, and Φ_{isc} (Table 4) for decay of the lowest-energy singlet excited state (S₁) are connected to the rate

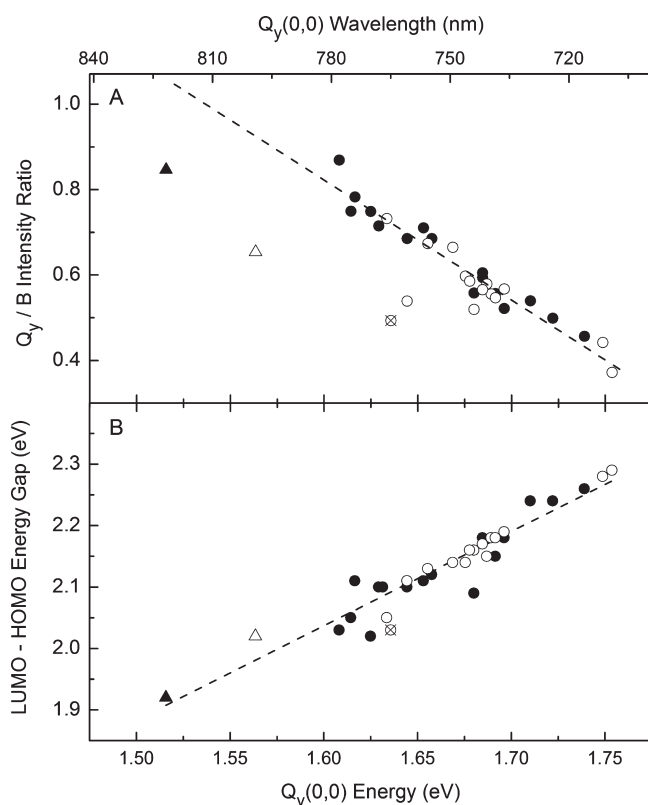


Figure 2. Integrated intensity ratio of the Q_y and B absorption manifolds versus (A) the $Q_y(0,0)$ absorption energy (and wavelength) and (B) the LUMO–HOMO energy gap. For both panels, the symbols designate the compounds as follows: S-H bacteriochlorins (closed circles), 5-OMe bacteriochlorins and bacteriooxophorbine (open circles), bacteriochlorinimides HBC-I (closed triangle) and MeOBC-I (open triangle), and photosynthetic pigment BPh *a* (open circle containing an “x”). The dashed line in each panel is the fit of the data for the synthetic bacteriochlorins and in (A) does not include the two bacteriochlorinimides.

constants for $S_1 \rightarrow S_0$ spontaneous fluorescence (k_f), $S_1 \rightarrow S_0$ internal conversion (k_{ic}), and $S_1 \rightarrow T_1$ intersystem crossing (k_{isc}) via eqs 1–3.

$$\tau_S = (k_f + k_{ic} + k_{isc})^{-1} \quad (1)$$

$$\Phi_f = k_f / (k_f + k_{ic} + k_{isc}) \quad (2)$$

$$\Phi_{isc} = k_{isc} / (k_f + k_{ic} + k_{isc}) \quad (3)$$

The internal conversion yield can be calculated from eq 4.

$$\Phi_{ic} = 1 - \Phi_f - \Phi_{isc} \quad (4)$$

The radiative, intersystem-crossing, and internal-conversion rate constants can be calculated from the above quantities via eq 5, where $i = f, isc$, or ic .

$$k_i = \Phi_i / \tau_S \quad (5)$$

The Φ_{ic} , k_f , k_{isc} , and k_{ic} values obtained using eqs 3–5, along with the measured values of τ_S , Φ_f and Φ_{isc} for the bacteriochlorins are given in Table 4.

The $S_1 \rightarrow S_0$ radiative rate constants are in the range $(18 \text{ ns})^{-1}$ to $(48 \text{ ns})^{-1}$. The rate constant for $S_1 \rightarrow S_0$ internal conversion is

in the range $(4 \text{ ns})^{-1}$ to $(27 \text{ ns})^{-1}$ and increases weakly with decreasing S_1 excited-state energy (based on the $Q_y(0,0)$ position), which is consistent with the energy-gap law for nonradiative decay.⁴⁵ The rate constant for $S_1 \rightarrow T_1$ intersystem crossing is in the range $(3 \text{ ns})^{-1}$ to $(18 \text{ ns})^{-1}$. The average values of k_f , k_{isc} , and k_{ic} for the HBC series are comparable to those for the MeOBC series.

6. Molecular Orbital Characteristics. To gain insight into the trends in the spectral and photophysical properties of the bacteriochlorins as a function of molecular characteristics, DFT calculations were performed.⁴² These calculations provide the energies and electron-density distributions of the frontier MOs. The principal orbitals of interest are the highest occupied molecular orbital (HOMO), the lowest unoccupied molecular orbital (LUMO), and the HOMO-1 and LUMO+1. The energies of these orbitals and various energy gaps relevant to the photophysical properties are given in Table 5. Table 6 shows electron-density plots of the MOs for representative bacteriochlorins.

The energies of the four frontier MOs are plotted as a function of the $Q_y(0,0)$ absorption-band wavelength/energy in Figure 4A, and analogous plots for the LUMO–HOMO energy gap and LUMO+1–HOMO-1 energy gap are shown in Figure 4B. In each of these plots, the data for bacteriochlorins containing 5-H and 5-OMe substituents are given by closed and open symbols, respectively. The data for the photosynthetic pigment BPh *a* are given by the open symbol containing an “x”. The HOMO–LUMO versus $Q_y(0,0)$ energy plot is reproduced in Figure 2B for direct comparison with the spectral data in Figure 2A (and the data for the two bacteriochlorinimides indicated by triangles). In analogy to Figure 4 for the $Q_y(0,0)$ band, the energies of the four frontier MOs are plotted as a function of the $Q_x(0,0)$ absorption-band wavelength/energy in Figure 5A, and analogous plots for the LUMO+1–HOMO energy gap and LUMO–HOMO-1 energy gap are shown in Figure 5B. The relationships depicted in these various plots are discussed as part of the spectral analysis given below.

DISCUSSION

The elucidation of the relationships between structural/MO characteristics and spectral/photophysical properties provides a foundation for the design of bacteriochlorins and extended analogues with desired properties for diverse applications. The variations in the MO characteristics reflect the nature and positions of the peripheral substituents on the bacteriochlorin. The MO characteristics in turn influence the photophysical properties (excited-state lifetimes and yields and rate constants of excited-state decay routes). The subsections below discuss the observed spectral and photophysical properties of the bacteriochlorins and the correlation of these properties with the calculated MO characteristics of the molecules.

1. General Characteristics of the $Q_y(0,0)$ Absorption Band. The $Q_y(0,0)$ transition is of particular interest because it corresponds to absorption of light to produce the lowest singlet excited state, which dominates much of the photophysical behavior. For applications, such behavior includes fluorescence (molecular imaging and flow cytometry) and energy/electron transfer (solar-energy conversion). Thus, understanding the impact of molecular factors that can be manipulated via synthesis is of great value toward the design of bacteriochlorins and related macrocycles with tunable properties.

Table 4. Photophysical Properties of Bacteriochlorins^a

compound	$Q_y(0,0)^b$ energy (cm ⁻¹)	τ_s^c (ns)	Φ_f^d	Φ_{isc}^e	Φ_{ic}^f	$(k_f)^{-1}g$ (ns)	$(k_{isc})^{-1}h$ (ns)	$(k_{ic})^{-1}i$ (ns)	τ_T^j (μ s)
HBC Series									
HBC-H	13996	4.0	0.14	0.62	0.24	29	6.5	17	169
HBC-Swt^{2,12}	13870	3.6	0.11	0.40	0.49	33	9.0	7	190
HBC-M^{3,13}	13774	3.5	0.15	0.65	0.20	23	5.4	18	233
HBC-Re^{3,13}	13624	3.0	0.08	0.56	0.36	38	5.4	8	198
HBC-F³	13615	3.4	0.12	0.80	0.08	28	4.2	42	66
HBC-T^{2,12}	13532	3.3	0.18	0.55	0.27	18	6.0	12	163
HBC-P^{3,13}	13532	3.3	0.13	0.68	0.19	25	4.9	17	118
HBC-C^{3,13 k}	13596	3.7	0.09	0.41	0.50	41	9.0	7	70
HBC-CN^{3,13}	13333	4.1	0.15	0.43	0.42	27	9.5	10	84
HBC-V^{3,13}	13298	3.3	0.17	0.55	0.28	19	6.0	12	108
HBC-MEs^{3,13}	13236	3.9	0.14	0.40	0.46	28	9.8	9	76
HBC-Me^{2,12}EEs^{3,13}	13123	3.0	0.13	0.52	0.35	23	5.8	9	64
HBC-Et^{2,12}EEs^{3,13}	13115	3.3	0.14	0.55	0.31	24	6.0	11	110
HBC-PB^{3,13}	13080	3.3	0.15	0.63	0.22	22	5.2	15	95
HBC-T^{2,12}EEs^{3,13}	12987	3.4	0.13	0.40	0.47	26	8.5	7	92
HBC-A^{3,13}	12996	2.9	0.11	0.49	0.40	26	5.9	7	55
HBC-F^{3,13}	12937	2.9	0.11	0.52	0.37	26	5.6	7	60
MeOBC Series									
MeOBC-H	14085	5.0	0.25	0.55	0.20	20	9.1	25	107
MeOBC-T^{2,12}	13633	4.5	0.20	0.42	0.38	23	10.7	12	107
MeOBC-Py^{3,13 k}	13560	4.0	0.13	0.51	0.36	31	7.8	11	96
MeOBC-EEs^{3,13}	13559	4.8	0.19	0.52	0.29	25	9.2	17	51
MeOBC-Me^{2,12}EEs^{3,13}	13523	4.4	0.17	0.53	0.30	26	8.3	15	85
MeOBC-Et^{2,12}EEs^{3,13}	13514	4.3	0.17	0.63	0.20	25	6.8	22	83
MeOBC-A^{3,13 k}	13441	3.8	0.14	0.48	0.38	27	7.9	10	38
MeOBC-Me^{2,12}A^{3,13 k}	13405	3.4	0.13	0.48	0.39	26	7.1	9	78
MeOBC-An^{2,12}EEs^{3,13}	13298	4.1	0.22	0.43	0.35	19	9.5	12	83
MeOBC-EEs^{2,3,12,13}	13141	4.3	0.16	0.24	0.60	27	17.9	7	46
15-Substituted Series									
MeOBC-OMe¹⁵	14124	6.2	0.16	0.71	0.13	39	8.7	48	103
MeOBC-T^{2,12}Bza¹⁵	13541	4.6	0.20	0.54	0.26	23	8.5	18	111
MeOBC-T^{2,12}PE^{15 k}	13219	5.3	0.19	0.62	0.19	28	8.5	28	96
Bacteriooxophorbine									
MeOBOP	13587	4.6	0.19	0.31	0.50	24	14.8	9	36
Bacteriochlorinimides									
MeOBC-I	12571	2.2	0.05	0.76	0.19	44	2.9	12	72
HBC-I	12188	1.9	0.04	0.51	0.45	48	3.7	4	85
Standard									
BPh a^l	13107	2.7	0.10	0.57	0.33	27	4.7	8	25

^a Measured in toluene at room temperature unless noted otherwise. ^b Average energy of the $Q_y(0,0)$ absorption and emission bands (Table 3). ^c Lifetime of the lowest singlet excited state measured using fluorescence techniques ($\pm 7\%$). ^d Fluorescence quantum yield ($\pm 5\%$). ^e Intersystem crossing (triplet) yield (± 0.09). ^f Internal conversion yield calculated via eq 4. ^g Inverse of the radiative (fluorescence) rate constant obtained via eq 5. ^h Inverse of the intersystem crossing rate constant obtained via eq 5. ⁱ Inverse of the internal conversion rate constant obtained via eq 5. ^j Lifetime of the lowest triplet excited state in Ar-purged 2-methyltetrahydrofuran measured via transient absorption spectroscopy ($\pm 10\%$). ^k Properties except Φ_{isc} measured in methanol. ^l Values in toluene. The values in ethanol are $\Phi_f = 0.081$, $\tau_s = 2.3$ ns, and $\tau_T = 30 \mu$ s. The values from ref 44 in acetone/methanol (7:3) are $\tau_s = 2.0$ ns, $\tau_s = 16 \mu$ s, and $\Phi_{isc} = 0.57$ (average of 0.54 and 0.60 from two methods).

The bacteriochlorins described herein span a large range of NIR positions of the $Q_y(0,0)$ absorption band (Figure 1 and Table 3), primarily due to the effects of 2,3,12,13-substituents (Tables 1 and 2). These positions are on the molecular y -axis, which is the axis along which the Q_y optical transition is polarized.

This fact is illustrated by the results of time-dependent DFT calculations for representative bacteriochlorins shown in Figure 6. These calculations show that the transition-dipole-moment direction for absorption to the lowest singlet excited state (the Q_y state) essentially bisects the pyrrole rings (which

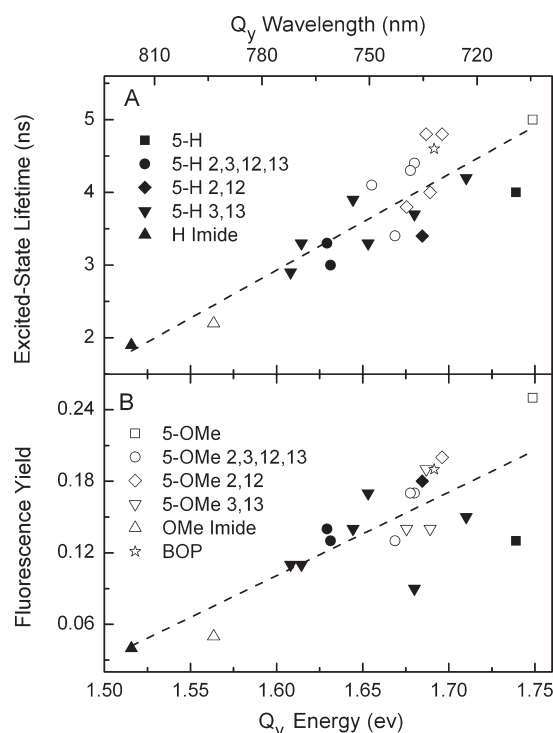


Figure 3. Singlet excited-state lifetime (τ_s) and fluorescence yield (Φ_s) versus the $Q_y(0,0)$ absorption energy (and wavelength) for representative bacteriochlorins, the bacteriochlorinimides, and MeOBOP (BOP). The closed symbols designate compounds containing a 5-H substituent, and the open symbol compounds contain a 5-OMe group. The open and closed symbols represent the same compounds in both panels, but the legends for one type (5-H vs 5-OMe) are shown in only one panel due to space limitations. The trend lines represent fits to all of the data shown in each panel.

contain the 2,3,12,13-positions). The $Q_y(0,0)$ band varies from 818 nm for imide **HBC-I** to 707 nm for **MeOBC-OMe**¹⁵. Analogues bearing a variety of 2,3,12,13-substituents, and with hydrogen or methoxy at the 5-position, provide coverage in relatively fine increments across the 700–800 nm spectral region (Figure 1).

Although there is significant tunability in the position of the $Q_y(0,0)$ absorption band (and in the analogous $Q_y(0,0)$ fluorescence band), the band retains its rather narrow bandwidth more or less independent of wavelength. The typical fwhm is 15 nm (Table 3). Such narrow absorption bandwidths are important for selective excitation in multicolor applications in optical molecular imaging or flow cytometry. The analogous narrow fluorescence bandwidths are similarly useful for selective detection in multichromophore imaging and cytometry protocols. For example, we have utilized these narrow bandwidths to illustrate the favorable properties of bacteriochlorins (in chlorin–bacteriochlorin dyads) versus common commercial dyes for optical molecular imaging^{15,16} including in mouse models.⁴⁶

2. Factors Affecting the Wavelength/Energy of the $Q_y(0,0)$ Absorption Band. The one-electron configuration resulting from light-induced promotion of an electron from the HOMO to the LUMO normally makes a significant contribution to the electronic characteristics of the lowest singlet excited state (S_1) of most molecules. According to Gouterman's four-orbital model,⁴⁷ this configuration as well as that derived from electron promotion

from the HOMO-1 to LUMO+1 define the wave function for the S_1 excited state and thus key characteristics (wavelength and intensity) of the $Q_y(0,0)$ absorption band of tetrapyrrole chromophores (including porphyrins, chlorins, and bacteriochlorins). We have previously applied this model to a series of about two dozen zinc chlorins.^{48–50}

In Gouterman's description, the HOMO → LUMO and HOMO-1 → LUMO+1 one-electron configurations make roughly equal contributions to the S_1 wave function for porphyrins, with a proportionately greater contribution of HOMO → LUMO configurations along the following series: porphyrin < chlorin < bacteriochlorin.⁴⁷ Indeed, time-dependent DFT calculations show that the S_1 excited state of bacteriochlorins is comprised of roughly 75% HOMO → LUMO, with most of the remainder due to HOMO-1 → LUMO+1. These contributions can be seen from the following examples: **HBC-H** (71%, 27%); **MeOBC-H** (71%, 28%); **MeOBOP** (73%, 25%); **HBC-I** (78%, 18%); **MeOBC-I** (76%, 20%); **MeOBC-A**^{3,13} (72%, 24%). These results are in keeping with those obtained from prior DFT⁵¹ and *ab initio*⁵² calculations.

The experimental results and MO calculations presented here are fully consistent with a dominant contribution of the HOMO → LUMO configuration for the bacteriochlorins and give insight into the underlying molecular origin. The slopes of the trend lines given in Figure 4A show that the LUMO ($m = 3.8$) is more strongly connected with the wavelength/energy of the $Q_y(0,0)$ absorption band than the HOMO ($m = 2.3$), LUMO+1 ($m = 2.9$), and HOMO-1 ($m = 2.8$). The slopes for the latter two orbitals are about equal. The result is a much greater magnitude of the slope of the trend line for the LUMO–HOMO energy gap ($m = 1.5$) versus the LUMO+1–HOMO-1 energy gap ($m = 0.09$) plotted against the $Q_y(0,0)$ wavelength/energy (Figure 4B). Consequently, the wavelength/position of the $Q_y(0,0)$ band is dominated by the LUMO–HOMO energy gap.

The greater dependence of the $Q_y(0,0)$ wavelength/energy on the LUMO (rather than the HOMO) can be traced to the generally greater electron density in the LUMO at the 2,3,12,13-positions, which are the locations of most of the substituents in the bacteriochlorins studied here (Tables 1, 2, and 6). [Note that for porphyrins the HOMO is an analogue of the HOMO-1 orbital of the bacteriochlorins, and thus the substituent effect on the LUMO–HOMO energy gap derives more from both orbitals rather than primarily from the LUMO.] For the molecules depicted in Table 6, these are the positions of the 2,12-*p*-tolyl groups of **HBC-T** and of the 3,13-carbonyl substituents (acetyl, ester, imide) of **MeOBC-A**^{3,13}, **MeOBC-I**, and **MeOBOP**. As noted above, the 2,3,12,13-positions are on the molecular *y*-axis, which is the axis on which the Q_y optical transition is polarized.

3. Effect of a 5-Methoxy Group on the Position of the $Q_y(0,0)$ Band. The 5-OMe group causes a hypsochromic shift in the $Q_y(0,0)$ band. The shifts in the (i) Q_y wavelength, (ii) Q_y energy, and (iii) LUMO–HOMO energy gap upon replacing 5-H with 5-OMe for six pairs of bacteriochlorins are as follows (Tables 3 and 5): **MeOBC-I** vs **HBC-I** (−25 nm, 0.05 eV, 0.10 eV); **MeOBCEtEs** vs **HBC-EtEs** (−22 nm, 0.05 eV, 0.06 eV); **MeOBCMeEs** vs **HBC-MeEs** (−22 nm, 0.05 eV, 0.06 eV); **MeOBC-A**^{3,13} vs **HBC-A**^{3,13} (−28 nm, 0.06 eV, 0.09 eV); **MeOBC-T**^{2,12} vs **HBC-T**^{2,12} (−5 nm, 0.01 eV, 0.01 eV); **MeOBC-H** vs **HBC-H** (−4 nm, 0.02 eV, 0.01 eV). The calculated shift in the MO energy gap parallels the observed shift in $Q_y(0,0)$ energy. There is a greater shift in both quantities

Table 5. Molecular Orbital Energies and Energy Gaps for Bacteriochlorins

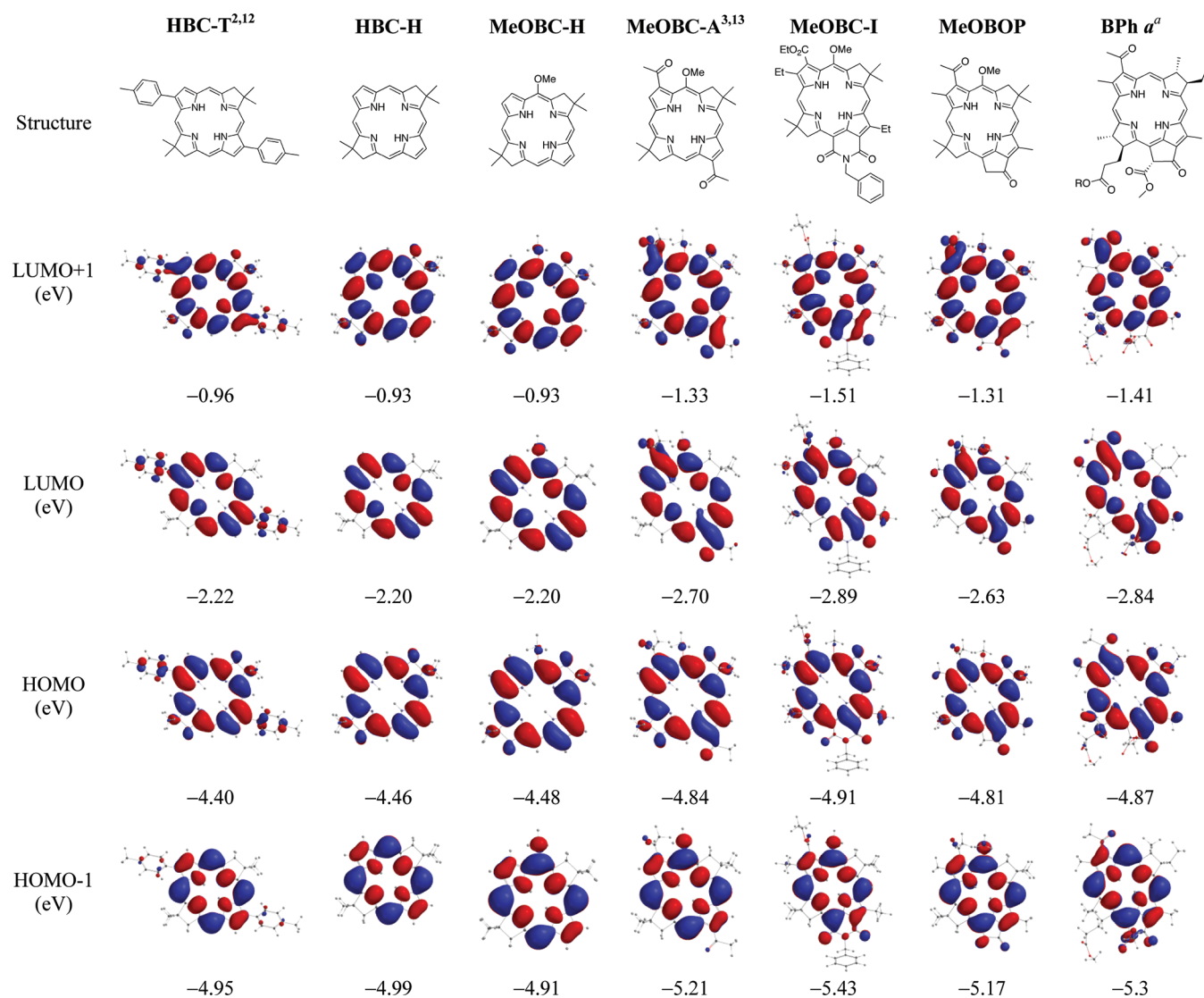
compound	HOMO-1 (eV)	HOMO (eV)	LUMO (eV)	LUMO+1 (eV)	LUMO-HOMO (eV)	LUMO+1-HOMO-1 (eV)	LUMO-HOMO-1 (eV)	LUMO+1-HOMO (eV)
HBC Series								
HBC-H	-4.99	-4.46	-2.20	-0.93	2.26	4.06	2.79	3.53
HBC-Swt ^{2,12}	-4.92	-4.36	-2.12	-0.89	2.24	4.03	2.8	3.47
HBC-M ^{3,13}	-4.98	-4.43	-2.19	-0.95	2.24	4.03	2.79	3.48
HBC-Re ^{3,13}	-5.01	-4.46	-2.28	-1.01	2.18	4.00	2.73	3.45
HBC-F ³	-5.21	-4.73	-2.58	-1.26	2.15	3.95	2.63	3.47
HBC-T ^{2,12}	-4.95	-4.40	-2.22	-0.96	2.18	3.99	2.73	3.44
HBC-P ^{3,13}	-5.00	-4.45	-2.28	-1.00	2.17	4.00	2.72	3.45
HBC-C ^{3,13}	-5.28	-4.86	-2.77	-1.30	2.09	3.98	2.51	3.56
HBC-CN ^{3,13}	-5.68	-5.22	-3.10	-1.65	2.12	4.03	2.58	3.57
HBC-V ^{3,13}	-5.03	-4.48	-2.37	-1.04	2.11	3.99	2.66	3.44
HBC-MEs ^{3,13}	-5.20	-4.77	-2.67	-1.21	2.10	3.99	2.53	3.56
HBC-Me ^{2,12} EEs ^{3,13}	-5.17	-4.67	-2.57	-1.19	2.1	3.98	2.6	3.48
HBC-Et ^{2,12} EEs ^{3,13}	-5.18	-4.68	-2.58	-1.20	2.10	3.98	2.60	3.48
HBC-PE ^{3,13}	-5.11	-4.53	-2.51	-1.17	2.02	3.94	2.60	3.36
HBC-T ^{2,12} EEs ^{3,13}	-5.27	-4.75	-2.64	-1.30	2.11	3.97	2.63	3.45
HBC-A ^{3,13}	-5.26	-4.83	-2.78	-1.31	2.05	3.95	2.48	3.52
HBC-F ^{3,13}	-5.41	-4.97	-2.94	-1.49	2.03	3.92	2.47	3.48
MeOBC Series								
MeOBC-H	-4.91	-4.48	-2.20	-0.93	2.28	3.98	2.71	3.55
MeOBC-T ^{2,12}	-4.88	-4.42	-2.23	-0.96	2.19	3.92	2.65	3.46
MeOBC-Py ^{3,13}	-5.21	-4.78	-2.60	-1.31	2.18	3.90	2.61	3.47
MeOBC-EEs ^{3,13}	-5.09	-4.75	-2.60	-1.21	2.15	3.88	2.49	3.54
MeOBC-Me ^{2,12} EEs ^{3,13}	-5.02	-4.61	-2.45	-1.12	2.16	3.90	2.57	3.49
MeOBC-Et ^{2,12} EEs ^{3,13}	-5.02	-4.60	-2.44	-1.11	2.16	3.91	2.58	3.49
MeOBC-A ^{3,13}	-5.21	-4.84	-2.70	-1.33	2.14	3.88	2.51	3.51
MeOBC-Me ^{2,12} A ^{3,13}	-5.12	-4.70	-2.56	-1.25	2.14	3.87	2.56	3.45
MeOBC-An ^{2,12} EEs ^{3,13}	-4.96	-4.56	-2.43	-1.08	2.13	3.88	2.53	3.48
MeOBC-EEs ^{2,3,12,13}	-5.32	-5.00	-2.95	-1.53	2.05	3.79	2.37	3.47
15-Substituted Series								
MeOBC-OMe ¹⁵	-4.84	-4.50	-2.21	-0.94	2.29	3.90	2.63	3.56
MeOBC-T ^{2,12} Bza ¹⁵	-4.89	-4.47	-2.30	-1.01	2.17	3.88	2.59	3.46
MeOBC-T ^{2,12} PE ¹⁵	-4.78	-4.51	-2.40	-1.18	2.11	3.60	2.38	3.33
Bacteriooxophorbine								
MeOBOP	-5.17	-4.81	-2.63	-1.31	2.18	3.86	2.54	3.5
Bacteriochlorinimides								
MeOBC-I	-5.43	-4.91	-2.89	-1.51	2.02	3.92	2.54	3.4
HBC-I	-5.51	-4.91	-2.99	-1.50	1.92	4.01	2.52	3.41
Standard								
BPh <i>a</i>	-5.30	-4.87	-2.84	-1.41	2.03	3.89	2.46	3.46

for compounds containing 3,13-dicarbonyl moieties (acetyl, ester, imide) compared to 3,13-diunsubstituted complex, even with 2,12-di-*p*-tolyl groups present. Furthermore, with no 2,3,12,13-substituents, the incorporation of a second meso-methoxy group in MeOBC-OMe¹⁵ (707 nm) gives a modest incremental hypsochromic shift of the Q_y(0,0) wavelength compared to one in MeOBC-H (709 nm), versus none in HBC-H (713 nm).

Close examination of the frontier MOs of the above-noted six pairs of compounds containing 5-OMe versus 5-H reveals an average effect on the orbital energies ($E_{5\text{-OMe}} - E_{5\text{-H}}$) in the

following order: HOMO (+0.01 eV) < LUMO+1 (+0.02 eV) < LUMO (+0.07 eV) < HOMO-1 (+0.10 eV). This ordering is consistent with the relative electron densities of the four frontier MOs at the 5-position (Table 6). These average orbital-energy values in turn give rise to average effects on the orbital-energy gaps ($\Delta E_{5\text{-OMe}} - \Delta E_{5\text{-H}}$) that are positive for the HOMO → LUMO configuration (+0.06 eV) and negative for the HOMO-1 → LUMO+1 (-0.08 eV). Given that the HOMO → LUMO configuration dominates the properties of the Q_y(0,0) band, these considerations correctly predict the hypsochromic shift

Table 6. Molecular-Orbital Energies and Electron-Density Distributions of Bacteriochlorins



^a Calculations for BPh *a* were performed with a truncated phytyl tail [$-\text{CH}_2-\text{CH}=\text{C}(\text{CH}_3)(\text{CH}_2\text{CH}_3)$], which is omitted in the display here.

(i.e., to higher energy) in the position of the band upon replacement of 5-H with 5-OMe. In turn, because the 5-OMe group does not strongly affect the HOMO energy, the spectral effect on the $\text{Q}_y(0,0)$ band derives primarily from the impact on the LUMO. Similar arguments should apply to bacteriochlorins with and without a 15-methoxy group and various 2,3,12,13-substituents because of the similar electron densities for each frontier MO at the 5- and 15-positions.

The effect of the 5-OMe group to reduce electron density in the bacteriochlorin π -system in the S_1 excited state is exacerbated by an increased contribution of the $\text{HOMO-1} \rightarrow \text{LUMO+1}$ configuration in the S_1 wave function within the four-orbital model. The $\text{LUMO+1}-\text{HOMO-1}$ energy gap is reduced and becomes closer to the $\text{LUMO}-\text{HOMO}$ energy gap (thereby increasing mixing of the two configurations), when a 5-OMe group is present (Table 5). This result derives primarily from the destabilizing effect of the 5-OMe group on the HOMO-1 orbital, which places considerable electron density at the 5 position and then onto the OMe group itself (Table 6).

The hypsochromic shift imparted by the 5-OMe group thus provides a design feature, along with placement of groups at the 2,3,12,13-positions, to obtain a palette of NIR absorbing bacteriochlorins with finely spaced bands. The 5-OMe group also allows modest control of excited-state lifetimes and fluorescence yields. This group also is quite useful for synthetic purposes in affording regioselective 15-bromination³⁰ and thereby enabling access to bacteriochlorinimides and a bacteriooxophorbine.³⁶

4. Intensity of the $\text{Q}_y(0,0)$ Absorption Band. Figure 2A shows that the $\text{Q}_y(0,0)$ band increases in relative intensity with a shift to longer wavelength (lower energy). In the four-orbital description, the Q_y -band intensity is related to the difference in energy of the $\text{LUMO}-\text{HOMO}$ and $\text{LUMO+1}-\text{HOMO-1}$ energy gaps.⁴⁷ As can be seen from Figure 4B, the $\text{LUMO}-\text{HOMO}$ energy gap changes substantially with $\text{Q}_y(0,0)$ wavelength/energy, whereas the $\text{LUMO+1}-\text{HOMO-1}$ energy gap does not. Thus, the intensity of the $\text{Q}_y(0,0)$ band is expected to track the $\text{LUMO}-\text{HOMO}$ energy gap, as is observed (Figure 2B). Because the $\text{LUMO}-\text{HOMO}$ energy gap also tracks the $\text{Q}_y(0,0)$

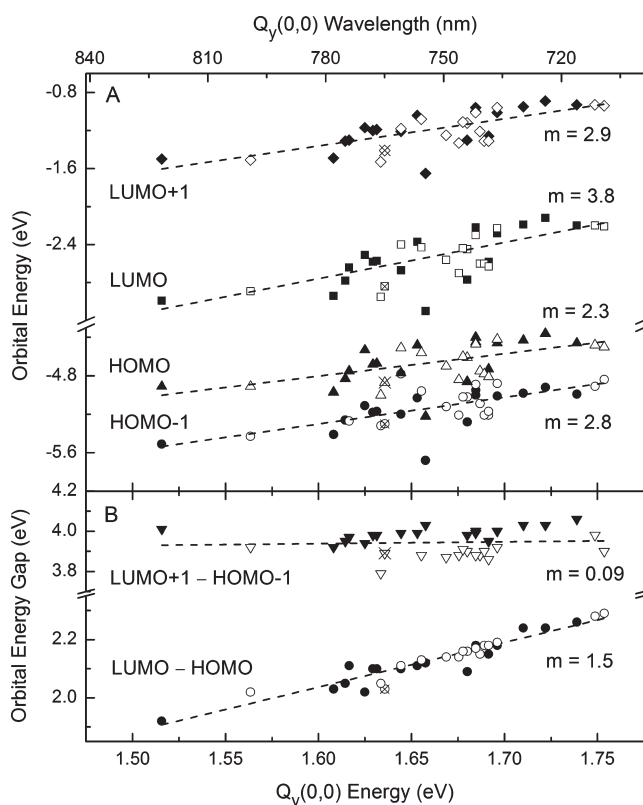


Figure 4. Molecular orbital energies (A) and energy gaps corresponding to the two y -polarized one-electron configurations (B) versus $Q_y(0,0)$ absorption energy (and wavelength). For each plot, the symbols designate the compounds as follows: 5-H bacteriochlorins and bacteriochlorinimide **HBC-I** (closed symbols); 5-OMe bacteriochlorins, bacteriochlorinimide **MeOBC-I**, and bacteriooxophorbine **MeOBOP** (open symbols); **BPh a** (open circle containing an “x”). The slopes (m) of the trendlines are shown.

wavelength/energy (Figure 4B), the positive correlation of $Q_y(0,0)$ energy/wavelength and intensity can be understood (Figure 2A). In turn, because the variation in LUMO–HOMO energy gap is associated substantially with the LUMO (Figure 4A), bacteriochlorin substituents that preferentially alter the LUMO versus HOMO energy (e.g., at the 2,3,12,13-positions) will change the intensity (like the wavelength) of the $Q_y(0,0)$ band in a predictable manner.

5. Position of the $Q_x(0,0)$ Absorption Band. The $Q_x(0,0)$ band reflects absorption to the second singlet excited state, which occurs in the blue-green spectral region (Figure 1 and Table 3). The analysis of substituent effects on the $Q_x(0,0)$ band closely parallels that given above concerning the $Q_y(0,0)$ band. The key findings are as follows: (i) The LUMO energy shows a much greater connection with $Q_x(0,0)$ energy/wavelength than the other frontier MOs (Figure 5A). (ii) Of the two electronic configurations that contribute to the Q_x wave function within the four-orbital model, the LUMO–HOMO-1 energy gap correlates with the $Q_x(0,0)$ energy/wavelength, while the LUMO+1–HOMO energy gap is essentially invariant (Figure 5B). (iii) It follows that the dependence of the LUMO on 2,3,12,13-substituents dominates the variation in the position of the $Q_x(0,0)$ band for the bacteriochlorins studied here, which again is derived from the generally greater electron density in the LUMO at these positions (Tables 1, 2, and 6). (iv) Similarly, because the intensity of the $Q_x(0,0)$ band, as reflected in the $Q_x(0,0)/Q_x(1,0)$

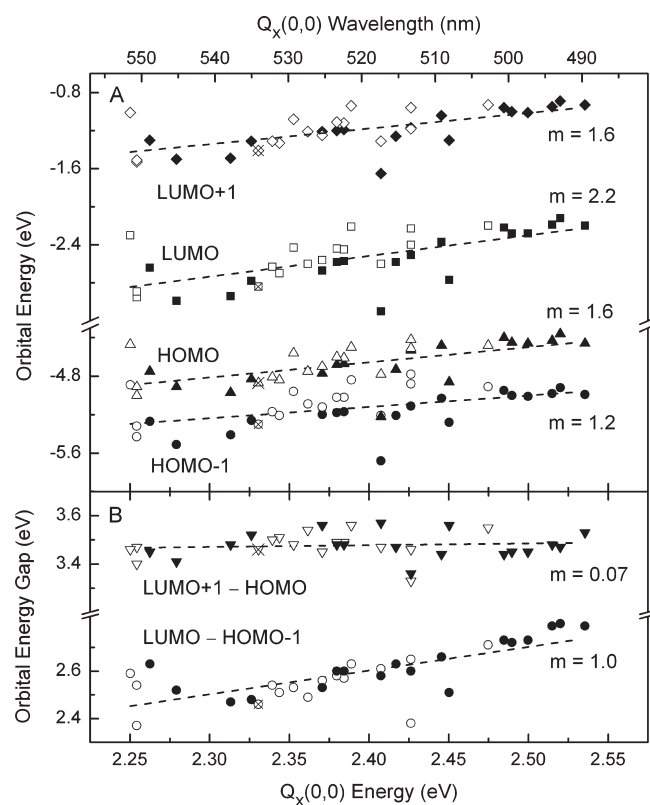


Figure 5. Frontier molecular orbital energies (A) and energy gaps corresponding to the two x -polarized one-electron configurations (B) versus $Q_x(0,0)$ absorption energy (and wavelength). For each plot, the symbols designate the compounds as follows: 5-H bacteriochlorins and bacteriochlorinimide **HBC-I** (closed symbols); 5-OMe bacteriochlorins, bacteriochlorinimide **MeOBC-I**, and bacteriooxophorbine **MeOBOP** (open symbols); **BPh a** (open circle containing an “x”). The slopes (m) of the trend lines are shown.

intensity ratio in Table 3, is expected to track the difference in the LUMO–HOMO-1 and LUMO+1–HOMO energy gaps, the $Q_x(0,0)$ intensity primarily tracks the LUMO–HOMO-1 gap and thus the LUMO energy. (v) The conclusion in (iii) along with the above-noted dominance of the LUMO in the substituent dependence of the $Q_y(0,0)$ band implies a correlation between the energy/wavelength of the two bands, as is observed (Figure 7). (vi) The offset parallel trend lines for bacteriochlorins containing 5-H substituents, 5-OMe groups, and 5,15-OMe (or 5-OMe plus the oxophorbine) (Figure 7) are related to the different (often reversed) effects of these substituents on the two bands (Table 3). For example, of the six pairs of bacteriochlorins that have a 5-OMe versus 5-H substituent, the greatest 5-OMe effect on the $Q_x(0,0)$ band is found for the $T^{2,12}$ compounds (a 12 nm bathochromic shift), whereas the greatest effect on the $Q_y(0,0)$ band is found for the carbonyl-containing ($-A^{3,13}$, -MeEs, -EtEs, imide) analogues (24–28 nm bathochromic shift). These differences are related to the electron densities in the MOs involved in the respective transitions.

6. Yields and Rate Constants of the Excited-State Decay Pathways. For all the (free base) bacteriochlorins under study, the average yields of fluorescence, intersystem crossing, and internal conversion are $\Phi_f = 0.15$, $\Phi_{isc} = 0.52$, and $\Phi_{ic} = 0.33$. The corresponding rate constants are $k_f = (27 \text{ ns})^{-1}$, $k_{isc} = (8 \text{ ns})^{-1}$, and $k_{ic} = (12 \text{ ns})^{-1}$, which are in concert with the average

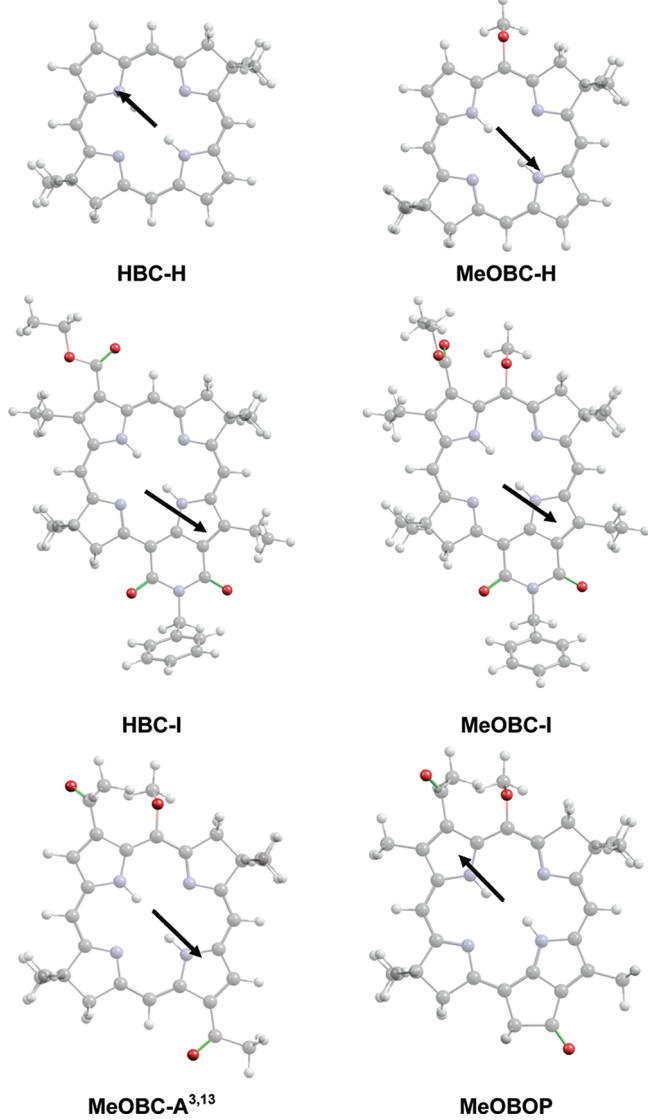


Figure 6. Transition-dipole-moment directions from time-dependent DFT calculations.

singlet excited-state lifetime of $\tau_S = 3.8$ ns. For comparison, values obtained from the photophysical data for free base *meso*-tetraphenylporphyrin are $\Phi_f = 0.10$, $\Phi_{isc} = 0.70$, $\Phi_{ic} = 0.20$, and $\tau_S = 13$ ns.^{39,53-56} Using eq 5, these values give corresponding rate constants of $k_f = (130 \text{ ns})^{-1}$, $k_{isc} = (19 \text{ ns})^{-1}$, and $k_{ic} = (65 \text{ ns})^{-1}$. The roughly 5-fold greater rate constant for $S_1 \rightarrow S_0$ (spontaneous) fluorescence (k_f) for bacteriochlorins versus porphyrins is paralleled by stronger (stimulated) $S_0 \rightarrow S_1$ absorption, namely, the integrated intensity of the Q_y absorption manifold [$Q_y(0,0)$, $Q_y(1,0)$, etc]; these two quantities are connected by the respective Einstein coefficients.

Although the yield for $S_1 \rightarrow T_1$ intersystem crossing is about 30% lower for bacteriochlorins versus porphyrins (0.5 versus 0.7), the rate constant for the process is about 2-fold greater [$(8 \text{ ns})^{-1}$ versus $(19 \text{ ns})^{-1}$]. Thus, spin-orbit coupling is actually enhanced in the bacteriochlorins versus porphyrins. Furthermore, the typical values of $\Phi_{\text{isc}} \sim 0.5$ for free base bacteriochlorins, along with triplet excited-state lifetimes of tens of microseconds to over one hundred microseconds (in the

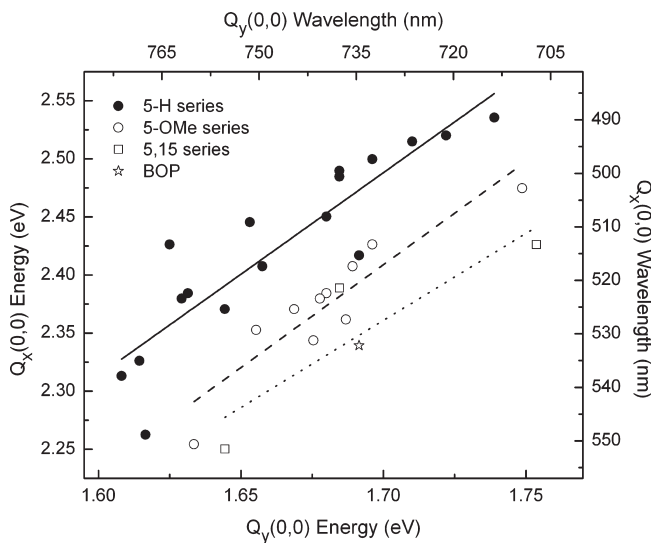


Figure 7. Energy (and wavelength) of the $Q_\infty(0,0)$ absorption band versus the energy (and wavelength) of the $Q_\infty(0,0)$ absorption band. The symbols designate the compounds as follows: 5-H bacteriochlorins (closed circles), 5-OMe bacteriochlorins (open circles), bacteriochlorins containing 5-OMe plus a 15-substituent (open squares), and bacteriooxophorbine MeOBOP (open star). The trend lines are fits to the data sets as follows: 5-H bacteriochlorins (solid), 5-OMe bacteriochlorins (dashed), 5,15-bacteriochlorins plus bacteriooxophorbine (dotted).

absence of O₂), is ample to support efficient sensitization in PDT,^{20–22} a process that is initiated via the triplet excited state. A key factor for the efficacy of the bacteriochlorins as PDT sensitizers is that their appropriate photophysical properties are coupled with (i) absorption in the NIR region, for which penetration into animal tissues is greater than for shorter wavelength (UV–vis) or longer wavelength (infrared) radiation, and (ii) the synthetic amenability to allow tailoring of the chromophores for cell uptake and delivery to diverse target sites.^{20–22}

Turning to the third decay process of the S_1 excited state, there is a 5-fold enhanced rate constant for $S_1 \rightarrow S_0$ internal conversion for bacteriochlorins versus the typical free base porphyrin [$(12 \text{ ns})^{-1}$ versus $(65 \text{ ns})^{-1}$]. There is also a modest, yet less dramatic, general increase in k_{ic} with decreasing S_1 [i.e., $Q_y(0,0)$] energy among the bacteriochlorins themselves (Table 4). These trends are expected on the basis of the energy-gap law for nonradiative decay.⁴⁵ In particular, the rate constant for internal conversion is expected to increase exponentially as the $S_1 - S_0$ energy gap decreases, via the typical energy-gap dependence of a Franck-Condon factor. Nonetheless, the average yield of the internal conversion process increases only from about 0.2 for free base porphyrins to 0.3 for the free base bacteriochlorins. Furthermore, the enhancement of this nonradiative decay process occurs to such a modest degree that the average bacteriochlorin singlet excited-state lifetime of ~ 4 ns is still quite long and more than sufficient to drive efficient energy/charge-transfer processes in solar energy and other applications. Relatively long S_1 lifetimes are retained even for the longest wavelength-absorbing bacteriochlorins studied here, namely, the bacteriochlorin-imides **MeOBC-I** ($\lambda_{Q_y(0,0)} = 793 \text{ nm}$; $\tau_S = 2.2 \text{ ns}$) and **HBC-I** ($\lambda_{Q_y(0,0)} = 818 \text{ nm}$; $\tau_S = 1.9 \text{ ns}$). These synthetic bacteriochlorins absorb at longer wavelength than the native photosynthetic free base bacteriochlorin **BPh a** (by ~ 40 and $\sim 70 \text{ nm}$, respectively).

yet have comparable excited-state lifetimes. Such characteristics bode well for the use of tunable synthetic bacteriochlorins to extend the properties available in the native photosynthetic pigments for diverse applications.

■ OUTLOOK

The studies reported herein delineate the spectral and photophysical properties of about three dozen synthetic bacteriochlorins and elucidate the origin of the variations in these properties as a function of substituent type and position on the macrocycle. The palette of synthetic bacteriochlorins represents a significant extension of the properties of the native photosynthetic pigments (bacteriochlorophylls). Understanding the design principles for tuning the spectral and photophysical characteristics establishes a path forward for utilizing the synthetic bacteriochlorins in a wide variety of photochemical applications. A result that deserves emphasis is that the wavelength tunability (achieved by introduction of diverse β -pyrrole substituents) stems largely from interaction of the auxochromes with the LUMO of the bacteriochlorin. The interaction of the auxochromes with the LUMO is also expected to alter the reduction potential with little effect on the oxidation potential of the bacteriochlorin. The lifetime of lowest singlet excited state (~ 2 to ~ 6 ns) augurs well for a wide variety of photochemical applications.

The types of applications that might be envisioned for the synthetic bacteriochlorins include the following:

- (1) Effective molecular imaging requires bright fluorophores in the NIR spectral region with avoidance of spectral overlap and light scattering. Brightness stems from the product of illumination intensity, absorption intensity, and fluorescence quantum yield; spectral overlap and light scattering are mitigated with sharp absorption/emission bands and relatively long excited-state lifetimes. The choice of NIR-active compound ultimately depends on a large number of factors including the aforementioned photophysical features as well as synthetic accessibility, solubility, toxicity, and amenability toward alteration of the molecular design. A malleable molecular design is essential, for example, to accommodate incorporation of diverse targeting agents. Versatility in molecular design depends in turn on the robustness of the synthetic plan and intrinsic features of the molecular architecture. While the diversity of NIR imaging applications undoubtedly requires diverse chromophores,^{19,20} the intrinsic photophysical features delineated herein and the molecular tailoring achieved to date (for the related topic of PDT)^{20–22} together indicate the synthetic bacteriochlorins appear well suited for such applications.
- (2) Enhanced sorting capabilities of cellular components require molecular tags with absorption that extends beyond the visible region. The strong and relatively narrow (as well as tunable) NIR absorption feature of the synthetic bacteriochlorins suggests utility as individually addressable dye markers in flow cytometry.
- (3) Enhanced capabilities for PDT applications require high triplet excited-state (intersystem crossing) yields. The synthetic bacteriochlorins exhibit this capability, in addition to the amenability toward synthetic tailoring for cell uptake and delivery to diverse target sites.
- (4) Efficient solar energy conversion requires the capability to capture NIR light because a significant fraction of the solar spectrum falls to the red of 600 nm. Bacteriochlorophyll

a and its metal free analogue BPh *a* typically absorb near 780 and 750 nm, respectively, as *monomers* in organic solvents yet exhibit longer wavelength absorption (e.g., 800, 850, 870 nm) in many native photosynthetic antenna systems owing to interactions between bacteriochlorophylls in oligomeric assemblies.¹ The synthetic free base bacteriochlorins reported herein extend the accessible spectral range as *monomers* to encompass ~ 700 to ~ 820 nm. The fine-tuning of the wavelength maximum of the lowest-energy absorption band across a significant portion of the NIR spectral region should enable enhanced collection of solar radiation and the design of energy-cascade systems wherein excitons are delivered in a controlled manner to a designated site. The wavelength tunability demonstrated here combined with the rich synthetic chemistry affords versatile building blocks for biomimetic construction of multipigment architectures in artificial photosynthesis and should facilitate the rational design of a wide variety of photochemical systems that function upon illumination in the NIR spectral region.

■ ASSOCIATED CONTENT

S Supporting Information. Synthesis procedures and characterization data for bacteriochlorin HBC-T^{2,12}EEs^{3,13}. This material is available free of charge via the Internet at <http://pubs.acs.org>.

■ AUTHOR INFORMATION

Corresponding Author

*E-mail: david.bocian@ucr.edu; jlindsey@ncsu.edu; holten@wustl.edu.

■ ACKNOWLEDGMENT

This work was supported by grants from the Division of Chemical Sciences, Geosciences, and Biosciences, Office of Basic Energy Sciences of the U.S. Department of Energy to DFB (DE-FG02-05ER15660), D.H. (DE-FG02-05ER15661), and JSI (DE-FG02-96ER14632). We thank the following individuals for contributing bacteriochlorins for photophysical analysis: Dr. Thiagarajan Balasubramanian, Dr. Eszter K. Borbas, Mr. Chih-Yuan Chen, Mr. David Cramer, Dr. Dazhong Fan, Dr. Brian E. McDowell, Dr. Marcin Ptaszek, and Dr. Christian Ruzié. We thank Dr. Hooi Ling Kee for photophysical measurements of several bacteriochlorins.

■ REFERENCES

- (1) Scheer, H. Chlorophylls and Bacteriochlorophylls. Biochemistry, Biophysics, Functions and Applications. *Advances in Photosynthesis and Respiration*; Grimm, B., Porra, R. J., Rüdiger, W., Scheer, H., Eds.; Springer: Dordrecht, The Netherlands, 2006; Vol. 25, pp 1–26.
- (2) (a) Ashur, I.; Goldschmidt, R.; Pinkas, I.; Salomon, Y.; Szewczyk, G.; Sarna, T.; Scherz, A. *J. Phys. Chem. A* **2009**, *113*, 8027–8037. (b) Kozyrev, A. N.; Chen, Y.; Goswami, L. N.; Tabaczynski, W. A.; Pandey, R. K. *J. Org. Chem.* **2006**, *71*, 1949–1960. (c) Limantara, L.; Koehler, P.; Wilhelm, B.; Porra, R. J.; Scheer, H. *Photochem. Photobiol.* **2006**, *82*, 770–780. (d) Vakrat-Haglili, Y.; Weiner, L.; Brumfeld, V.; Brandis, A.; Salomon, Y.; McIlroy, B.; Wilson, B. C.; Pawlak, A.; Rozanowska, M.; Sarna, T.; Scherz, A. *J. Am. Chem. Soc.* **2005**, *127*, 6487–6497. (e) Fiedor, J.; Fiedor, L.; Kammerhuber, N.; Scherz, A.; Scheer, H. *Photochem. Photobiol.* **2002**, *76*, 145–152.

- (3) Grin, M. A.; Mironov, A. F.; Shtil, A. A. *Anti-Cancer Agents Med. Chem.* **2008**, *8*, 683–697.
- (4) Chen, Y.; Li, G.; Pandey, R. K. *Curr. Org. Chem.* **2004**, *8*, 1105–1134.
- (5) Galezowski, M.; Gryko, D. T. *Curr. Org. Chem.* **2007**, *11*, 1310–1338.
- (6) (a) Aratani, N.; Osuka, A. In *Handbook of Porphyrin Science*; Kadish, K. M., Smith, K. M., Guilard, R., Eds.; World Scientific Publishing Co.: Singapore, 2010; Vol. 1, pp 1–132. (b) Maretina, I. A. *Russ. J. Gen. Chem.* **2009**, *79*, 1544–1581. (c) Flamigni, L. *J. Photochem. Photobiol. C: Photochem. Rev.* **2007**, *8*, 191–210. (d) Iengo, E.; Scandola, F.; Alessio, E. *Struct. Bonding (Berlin)* **2006**, *121*, 105–143. (e) Harvey, P. D. In *The Porphyrin Handbook*; Kadish, K. M., Smith, K. M., Guilard, R., Eds.; Academic Press: San Diego, CA, 2003; Vol. 18, pp 63–250. (f) Holten, D.; Bocian, D. F.; Lindsey, J. S. *Acc. Chem. Res.* **2002**, *35*, 57–69. (g) Gust, D.; Moore, T. A. In *The Porphyrin Handbook*; Kadish, K. M., Smith, K. M., Guilard, R., Eds.; Academic Press: San Diego, CA, 2000; Vol. 8, pp 153–190. (h) Gribkova, S. E.; Evstigneeva, R. P.; Luzgina, V. N. *Russ. Chem. Rev.* **1993**, *62*, 963–979. (i) Wasielewski, M. R. *Chem. Rev.* **1992**, *92*, 435–461. (j) Wasielewski, M. R. In *Chlorophylls*; Scheer, H., Ed.; CRC Press: Boca Raton, FL, USA, 1991; pp 269–286.
- (7) Lindsey, J. S.; Mass, O.; Chen, C.-Y. *New J. Chem.* **2011**, *35*, 511–516.
- (8) Kobayashi, M.; Akiyama, M.; Kano, H.; Kise, H. In *Chlorophylls and Bacteriochlorophylls: Biochemistry, Biophysics, Functions and Applications*; Grimm, B., Porra, R. J., Rüdiger, W., Scheer, H., Eds.; Springer: Dordrecht, The Netherlands, 2006; pp 79–94.
- (9) Stromberg, J. R.; Marton, A.; Kee, H. L.; Kirmaier, C.; Diers, J. R.; Muthiah, C.; Taniguchi, M.; Lindsey, J. S.; Bocian, D. F.; Meyer, G. J.; Holten, D. *J. Phys. Chem. C* **2007**, *111*, 15464–15478.
- (10) (a) Chattopadhyay, P. K.; Hogerkorp, C.-M.; Roederer, M. *Immunology* **2008**, *125*, 441–449. (b) Shapiro, H. M. In *Flow Cytometry for Biotechnology*; Sklar, L. A., Ed.; Oxford University Press: NY, pp 15–39.
- (11) Sutton, J. M.; Clarke, O. J.; Fernandez, N.; Boyle, R. W. *Bioconjugate Chem.* **2002**, *13*, 249–263.
- (12) Ethirajan, M.; Chen, Y.; Joshi, P.; Pandey, R. K. *Chem. Soc. Rev.* **2011**, *40*, 340–362.
- (13) Singh, S.; Aggarwal, A.; Thompson, S.; Tomé, J. P. C.; Zhu, X.; Samaroo, D.; Vinod, M.; Gao, R.; Drain, C. M. *Bioconjugate Chem.* **2010**, *21*, 2136–2146.
- (14) Cao, W.; Ng, K. K.; Corbin, I.; Zhang, Z.; Ding, L.; Chen, J.; Zheng, G. *Bioconjugate Chem.* **2009**, *20*, 2023–2031.
- (15) Kee, H. L.; Diers, J. R.; Ptaszek, M.; Muthiah, C.; Fan, D.; Lindsey, J. S.; Bocian, D. F.; Holten, D. *Photochem. Photobiol.* **2009**, *85*, 909–920.
- (16) Kee, H. L.; Nothdurft, R.; Muthiah, C.; Diers, J. R.; Fan, D.; Ptaszek, M.; Bocian, D. F.; Lindsey, J. S.; Culver, J. P.; Holten, D. *Photochem. Photobiol.* **2008**, *84*, 1061–1072.
- (17) Akers, W.; Lesage, F.; Holten, D.; Achilefu, S. *Mol. Imaging* **2007**, *6*, 237–246.
- (18) Frangioni, J. V. *Curr. Opin. Chem. Biol.* **2003**, *7*, 626–634.
- (19) Licha, K. *Top. Curr. Chem.* **2002**, *222*, 1–29.
- (20) Mroz, P.; Huang, Y.-Y.; Szokalska, A.; Zhiyentayev, T.; Janjua, S.; Nifli, A.-P.; Sherwood, M. E.; Ruzié, C.; Borbas, K. E.; Fan, D.; Krayer, M.; Balasubramanian, T.; Yang, E.; Kee, H. L.; Kirmaier, C.; Diers, J. R.; Bocian, D. F.; Holten, D.; Lindsey, J. S.; Hamblin, M. R. *FASEB J.* **2010**, *24*, 3160–3170.
- (21) Huang, Y.-Y.; Mroz, P.; Zhiyentayev, T.; Sharma, S. K.; Balasubramanian, T.; Ruzié, C.; Krayer, M.; Fan, D.; Borbas, K. E.; Yang, E.; Kee, H. L.; Kirmaier, C.; Diers, J. R.; Bocian, D. F.; Holten, D.; Lindsey, J. S.; Hamblin, M. R. *J. Med. Chem.* **2010**, *53*, 4018–4027.
- (22) Huang, L.; Huang, Y.-Y.; Mroz, P.; Tegos, G. P.; Zhiyentayev, T.; Sharma, S. K.; Lu, Z.; Balasubramanian, T.; Krayer, M.; Ruzié, C.; Yang, E.; Kee, H. L.; Kirmaier, C.; Diers, J. R.; Bocian, D. F.; Holten, D.; Lindsey, J. S.; Hamblin, M. R. *Antimicrob. Agents Chemother.* **2010**, *54*, 3834–3841.
- (23) O'Connor, A. E.; Gallagher, W. M.; Byrne, A. T. *Photochem. Photobiol.* **2009**, *85*, 1053–1074.
- (24) Brandis, A. S.; Salomon, Y.; Scherz, A. In *Chlorophylls and Bacteriochlorophylls: Biochemistry, Biophysics, Functions and Applications*; Grimm, B., Porra, R. J., Rüdiger, W., Scheer, H., Eds.; Springer: Dordrecht, The Netherlands, 2006; pp 485–494.
- (25) Nyman, E. S.; Hynninen, P. H. *J. Photochem. Photobiol. B: Biol.* **2004**, *73*, 1–28.
- (26) Bonnett, R. *Chemical Aspects of Photodynamic Therapy*; Gordon and Breach Science Publishers: Amsterdam, 2000.
- (27) Davis, N. K. S.; Thompson, A. L.; Anderson, H. L. *J. Am. Chem. Soc.* **2011**, *133*, 30–31.
- (28) Ikeda, S.; Togano, M.; Eswaramoorthi, S.; Lim, J. M.; Kim, D.; Furuta, H. *J. Org. Chem.* **2010**, *75*, 8637–8649.
- (29) Kim, H.-J.; Lindsey, J. S. *J. Org. Chem.* **2005**, *70*, 5475–5486.
- (30) Fan, D.; Taniguchi, M.; Lindsey, J. S. *J. Org. Chem.* **2007**, *72*, 5350–5357.
- (31) McDowell, B. E. Ph.D. thesis, North Carolina State University, 2007.
- (32) Taniguchi, M.; Cramer, D. L.; Bhise, A. D.; Kee, H. L.; Bocian, D. F.; Holten, D.; Lindsey, J. S. *New J. Chem.* **2008**, *32*, 947–958.
- (33) Borbas, K. E.; Ruzié, C.; Lindsey, J. S. *Org. Lett.* **2008**, *10*, 1931–1934.
- (34) Ruzié, C.; Krayer, M.; Balasubramanian, T.; Lindsey, J. S. *J. Org. Chem.* **2008**, *73*, 5806–5820.
- (35) Krayer, M.; Ptaszek, M.; Kim, H.-J.; Meneely, K. R.; Fan, D.; Secor, K.; Lindsey, J. S. *J. Org. Chem.* **2010**, *75*, 1016–1039.
- (36) Krayer, M.; Yang, E.; Diers, J. R.; Bocian, D. F.; Holten, D.; Lindsey, J. S. *New J. Chem.* **2011**, *35*, 587–601.
- (37) Kee, H. L.; Bhaumik, J.; Diers, J. R.; Mroz, P.; Hamblin, M. R.; Bocian, D. F.; Lindsey, J. S.; Holten, D. *J. Photochem. Photobiol. A: Chem.* **2008**, *200*, 346–355.
- (38) Seybold, P. G.; Gouterman, M. *J. Mol. Spectrosc.* **1969**, *31*, 1–13.
- (39) Gradyushko, A. T.; Sevchenko, A. N.; Solovyov, K. N.; Tsvirk, M. P. *Photochem. Photobiol.* **1970**, *11*, 387–400.
- (40) Weber, G.; Teale, F. W. J. *Trans. Faraday Soc.* **1957**, *53*, 646–655.
- (41) Kee, H. L.; Kirmaier, C.; Yu, L.; Thamyonkit, P.; Youngblood, W. J.; Calder, M. E.; Ramos, L.; Noll, B. C.; Bocian, D. F.; Scheidt, W. R.; Birge, R. R.; Lindsey, J. S.; Holten, D. *J. Phys. Chem. B* **2005**, *109*, 20433–20443.
- (42) Except for molecular mechanics and semi-empirical models, the calculation methods used in Spartan have been documented in: Shao, Y.; Molnar, L. F.; Jung, Y.; Kussmann, J.; Ochsenfeld, C.; Brown, S. T.; Gilbert, A. T. B.; Slipchenko, L. V.; Levchenko, S. V.; O'Neill, D. P.; et al. *Phys. Chem. Chem. Phys.* **2006**, *8*, 3172–3191.
- (43) Smith, J. H. C.; Benitez, A. In *Modern Methods of Plant Analysis*; Paech, K., Tracey, M. V., Eds.; Springer-Verlag: Berlin, 1955; Vol. IV, pp 142–196.
- (44) Holten, D.; Gouterman, M.; Parson, W. W.; Windsor, M. W.; Rockley, M. G. *Photochem. Photobiol.* **1976**, *23*, 415–423.
- (45) Birks, J. B. *Photophysics of Aromatic Molecules*; Wiley-Interscience: London, 1970; pp 140–192.
- (46) Ptaszek, M.; Kee, H. L.; Muthiah, C.; Nothdurft, R.; Akers, W.; Achilefu, S.; Culver, J. P.; Holten, D. *Proc. SPIE* **2010**, *7576*, 75760E1–11.
- (47) (a) Gouterman, M. In *The Porphyrins*; Dolphin, D., Ed.; Academic Press: New York, 1978; Vol. 3, pp 1–165. (b) Gouterman, M. *J. Mol. Spectrosc.* **1961**, *6*, 138–163. (c) Gouterman, M. *J. Chem. Phys.* **1959**, *30*, 1139–1161.
- (48) Kee, H. L.; Kirmaier, C.; Tang, Q.; Diers, J. R.; Muthiah, C.; Taniguchi, M.; Laha, J. K.; Ptaszek, M.; Lindsey, J. S.; Bocian, D. F.; Holten, D. *Photochem. Photobiol.* **2007**, *83*, 1110–1124.
- (49) Kee, H. L.; Kirmaier, C.; Tang, Q.; Diers, J. R.; Muthiah, C.; Taniguchi, M.; Laha, J. K.; Ptaszek, M.; Lindsey, J. S.; Bocian, D. F.; Holten, D. *Photochem. Photobiol.* **2007**, *83*, 1125–1143.
- (50) Mass, O.; Ptaszek, M.; Taniguchi, M.; Diers, J. R.; Kee, H. L.; Bocian, D. F.; Holten, D.; Lindsey, J. S. *J. Org. Chem.* **2009**, *74*, 5276–5289.
- (51) (a) Linnanto, J.; Korppi-Tommola, J. *Phys. Chem. Chem. Phys.* **2006**, *8*, 663–687. (b) Petit, L.; Quartarolo, A.; Adamo, C.; Russo, N. *J. Phys. Chem. B* **2006**, *110*, 2398–2404.

- (52) (a) Petke, J. D.; Maggiora, G. M.; Shipman, L. L.; Christoffersen, R. E. *Photochem. Photobiol.* **1980**, *32*, 399–414. (b) Weiss, C., Jr. *J. Mol. Spectrosc.* **1972**, *44*, 37–80.
- (53) Yang, S. I.; Seth, J.; Strachan, J.-P.; Gentemann, S.; Kim, D.; Holten, D.; Lindsey, J. S.; Bocian, D. F. *J. Porphyrins Phthalocyanines* **1999**, *3*, 117–147.
- (54) Kikuchi, K.; Kurabayashi, Y.; Kokubun, H.; Kaizu, Y.; Kobayashi, H. *J. Photochem. Photobiol. A: Chem.* **1988**, *45*, 261–263.
- (55) Kajii, Y.; Obi, K.; Tanaka, I.; Tobita, S. *Chem. Phys. Lett.* **1984**, *111*, 347–349.
- (56) Bonnett, R.; McGarvey, D. J.; Harriman, A.; Land, E. J.; Truscott, T. G.; Winfield, U.-J. *Photochem. Photobiol.* **1988**, *48*, 271–276.